The Astrophysical Journal, 878:73 (8pp), 2019 June 10 https://doi.org/10.3847/1538-4357/ab0d22

ALMA 26 arcmin^2 Survey of GOODS-S at 1 mm (ASAGAO): Near-infrared-dark Faint ALMA Sources

Yuki Yamaguchi[1], Kotaro Kohno[1,2], Bunyo Hatsukade[1], Tao Wang[1,3], Yuki Yoshimura[1], Yiping Ao[4], Karina I. Caputi[5], James S. Dunlop[6], Eiichi Egami[7], Daniel Espada[3,8], Seiji Fujimoto[9], Natsuki H. Hayatsu[10,11], Rob J. Ivison[6,11], Tadayuki Kodama[12], Haruka Kusakabe[13], Tohru Nagao[14], Masami Ouchi[9,15], Wiphu Rujopakarn[15,16,17], Ken-ichi Tadaki[3], Yoichi Tamura[18], Yoshihiro Ueda[19], Hideki Umehata[1,20], Wei-Hao Wang[21,22], and Min S. Yun[23]

[1] Institute of Astronomy, Graduate School of Science, The University of Tokyo, 2-21-1 Osawa, Mitaka, Tokyo 181-0015, Japan; yyamaguchi@ioa.s.u-tokyo.ac.jp
[2] Research Center for the Early Universe, Graduate School of Science, The University of Tokyo, 7-3-1, Hongo, Bunkyo, Tokyo 113-0033, Japan
[3] National Astronomical Observatory of Japan, 2-21-1 Osawa, Mitaka, Tokyo 181-8588, Japan
[4] Purple Mountain Observatory and Key Laboratory for Radio Astronomy, Chinese Academy of Sciences, 8 Yuanhua Road, Nanjing 210034, People's Republic of China
[5] Kapteyn Astronomical Institute, University of Groningen, P.O. Box 800, 9700AV Groningen, The Netherlands
[6] Institute for Astronomy, University of Edinburgh, Royal Observatory, Edinburgh EH9 3HJ, UK
[7] Steward Observatory, University of Arizona, 933 North Cherry Avenue, Tucson, AZ 85721, USA
[8] Department of Astronomical Science, SOKENDAI (The Graduate University of Advanced Studies), 2-21-1 Osawa, Mitaka, Tokyo 181-8588, Japan
[9] Institute for Cosmic Ray Research, The University of Tokyo, Kashiwa, Chiba 277-8582, Japan
[10] Department of Physics, Graduate School of Science, The University of Tokyo, 7-3-1 Hongo, Bunkyo, Tokyo 113-0033, Japan
[11] European Southern Observatory, Karl-Schwarzschild-Str. 2, D-85748 Garching, Germany
[12] Astronomical Institute, Tohoku University, 6-3 Aramaki, Aoba, Sendai, Miyagi 980-8578, Japan
[13] Department of Astronomy, Graduate School of Science, The University of Tokyo, 7-3-1 Hongo, Bunkyo, Tokyo 113-0033, Japan
[14] Research Center for Space and Cosmic Evolution, Ehime University, 2-5 Bunkyo-cho, Matsuyama, Ehime 790-8577, Japan
[15] Kavli Institute for the Physics and Mathematics of the Universe (Kavli IPMU), WPI, The University of Tokyo, Kashiwa, Chiba 277-8583, Japan
[16] Department of Physics, Faculty of Science, Chulalongkorn University, 254 Phayathai Road, Pathumwan, Bangkok 10330, Thailand
[17] National Astronomical Research Institute of Thailand (Public Organization), Don Kaeo, Mae Rim, Chiang Mai 50180, Thailand
[18] Division of Particle and Astrophysical Science, Nagoya University, Furocho, Chikusa, Nagoya 464-8602, Japan
[19] Department of Astronomy, Kyoto University, Kyoto 606-8502, Japan
[20] RIKEN Cluster for Pioneering Research, 2-1 Hirosawa, Wako-shi, Saitama 351-0198, Japan
[21] Academia Sinica Institute of Astronomy and Astrophysics (ASIAA), No. 1, Sec. 4, Roosevelt Rd., Taipei 10617, Taiwan
[22] Canada–France–Hawaii Telescope (CFHT), 65-1238 Mamalahoa Highway, Kamuela, HI 96743, USA
[23] Department of Astronomy, University of Massachusetts, Amherst, MA 01003, USA
Received 2018 November 30; revised 2019 February 12; accepted 2019 March 4; published 2019 June 14

Abstract

We report detections of two 1.2 mm continuum sources ($S_{1.2\,\mathrm{mm}} \sim 0.6$ mJy) without any counterparts in the deep *H*- and/or *K*-band image (i.e., *K*-band magnitude $\gtrsim$26 mag). These near-infrared-dark faint millimeter sources are uncovered by ASAGAO, a deep and wide-field ($\simeq$26 arcmin^2) Atacama Large Millimeter/submillimeter Array (ALMA) 1.2 mm survey. One has a red IRAC (3.6 and 4.5 μm) counterpart, and the other has been independently detected at 850 and 870 μm using SCUBA2 and ALMA Band 7, respectively. Their optical-to-radio spectral energy distributions indicate that they can lie at $z \gtrsim 3$–5 and can be in the early phase of massive galaxy formation. Their contribution to the cosmic star formation rate density is estimated to be $\sim 1 \times 10^{-3}\,M_{\odot}\,\mathrm{yr}^{-1}\,\mathrm{Mpc}^{-3}$ if they lie somewhere in the redshift range of $z \sim 3$–5. This value can be consistent with, or greater than, that of bright submillimeter galaxies ($S_{870\,\mu\mathrm{m}} > 4.2$ mJy) at $z \sim 3$–5. We also uncover three more candidate near-infrared-dark faint ALMA sources without any counterparts ($S_{1.2\,\mathrm{mm}} \sim 0.45$–0.86 mJy). These results show that an unbiased ALMA survey can reveal the dust-obscured star formation activities, which were missed in previous deep optical/near-infrared surveys.

Key words: galaxies: evolution – galaxies: high-redshift – galaxies: star formation – submillimeter: galaxies

1. Introduction

The advent of the Atacama Large Millimeter/submillimeter Array (ALMA), which offers high sensitivity and angular resolution capabilities, has enabled us to uncover faint (sub) millimeter populations (observed flux densities, $S_{\mathrm{obs}} \simeq 0.1$–1 mJy, corresponding to infrared luminosity of $L_{\mathrm{IR}} \lesssim 10^{12}\,L_{\odot}$[24]). Recently, several blind surveys using ALMA have been performed in the SXDF (e.g., Tadaki et al. 2015; Hatsukade et al. 2016; Kohno et al. 2016; Wang et al. 2016; Yamaguchi et al. 2016) and the GOODS-S field (Aravena et al. 2016; Dunlop et al. 2017; Franco et al. 2018; Fujimoto et al. 2018; Hatsukade et al. 2018; Ueda et al. 2018, Yamaguchi et al. 2019) to detect and characterize the faint (sub) millimeter galaxies (hereafter, faint SMGs). These studies suggest that they are primarily "typical" or "the main-sequence" star-forming galaxies at $z = 1$–4 (e.g., da Cunha et al. 2015; Aravena et al. 2016; Yamaguchi et al. 2016; Dunlop et al. 2017, Yamaguchi et al. 2019), based on the cross-matching of the ALMA-selected sources and optical-to near-infrared-selected sources with reliable photometric redshifts and stellar mass estimates.

Here, we focus on the ALMA-selected galaxies that are not well characterized by such a cross-matching technique, i.e., faint SMGs without significant counterpart seen in the optical

[24] Rest-frame 8–1000 μm.

and near-infrared (near-IR) wavelengths. The existence of optical/near-IR-dark SMGs have already been reported by using pre-ALMA interferometers (e.g., Yun et al. 2008; Wang et al. 2009; Tamura et al. 2010). In the ALMA era, Simpson et al. (2014) found that a significant fraction (17 out of 96) of the bright ALMA sources in ECDF-S, which are originally selected by the LABOCA on APEX survey at 870 μm, are too faint in the optical/near-IR bands to obtain reliable constraints on their photometric redshift, arguing that such "near-IR-dark" SMGs tend to lie at higher redshift than the typical SMGs based on the *Herschel* stacking. Similarly, ALMA follow-up observations of SCUBA2-selected SMGs in UDS revealed that 4 bright ALMA sources out of 23 does not have significant near-IR counterparts (Simpson et al. 2015). And in fact, such trend extends to the faint SMGs purely selected by ALMA. For instance, Fujimoto et al. (2016) suggest that $\simeq$40% of faint ALMA sources ($S_{1.2\,\mathrm{mm}} = 0.02$–1 mJy) uncovered in the ALMA archival images of various fields (the total coverage is $\sim$9 arcmin^2) have no counterparts at optical/near-IR wavelengths (the 5σ limiting magnitude of $\sim$27–28 mag at optical wavelengths and $\sim$25–26 mag at near-IR wavelengths). Yamaguchi et al. (2016) find that one out of five ALMA sources in the 2 arcmin^2 survey of SXDF ($S_{1.1\,\mathrm{mm}} = 0.54$–2.0 mJy) are faint at *H*-band ($\simeq$25.3 mag) and not detected at wavelengths shorter than $\sim$1.3 μm. All these studies strongly motivate us to conduct a systematic search for near-IR-dark faint SMGs in the fields where the deepest near-IR images to date are available.

In this paper, we report detections of near-IR-dark, faint ALMA sources ($S_{1.2\,\mathrm{mm}} = 0.45$–0.86 mJy), which do not have any significant counterparts in the ultra-deep *H*- and/or *K*-band images, based on the ALMA twenty Six Arcmin^2 survey of GOODS-S At One-millimeter (ASAGAO; Project ID: 2015.1.00098.S, PI: K. Kohno). This paper is structured as follows. Section 2 presents ALMA observations and ALMA source identification. In Section 3, we describe the properties of the near-IR-dark faint ALMA sources detected by ASAGAO. Then, we put constraints on their physical properties such as redshifts and stellar masses in Section 4. Finally, we estimate their contribution to the cosmic star formation rate density (SFRD) in the high-redshift universe (Section 5). Throughout this paper, we assume a Λ cold dark matter cosmology with $\Omega_\mathrm{M} = 0.3$, $\Omega_\Lambda = 0.7$, and $H_0 = 70\,\mathrm{km\,s^{-1}\,Mpc^{-1}}$. All magnitude are given according to the AB system. We adopt the Chabrier Initial Mass Function (IMF; Chabrier 2003) when necessary to compute the SFR in galaxies in this paper.

2. ALMA Source Catalog and Identifications of Near-IR-dark Faint ALMA Candidates

We examined 25 secure ALMA sources with signal-to-noise ratio (S/N) > 5 in the 26 arcmin^2 map of the ASAGAO (Hatsukade et al. 2018) to search for near-IR dark faint ALMA sources. Here we adopt peak S/N values, rather than the spatially integrated S/N values, to conduct source extraction. The details of the ALMA observations and the source catalog creation are given in Hatsukade et al. (2018). Here we provide a brief overview. The 26 arcmin^2 map of the ASAGAO field was obtained at 1.14 and 1.18 mm (two tunings) to cover a wider frequency range, whose central wavelength was 1.16 mm. To obtain the best ALMA image of this field, we also include ALMA archival data toward the same field (Project ID: 2015.1.00543.S, PI: D. Elbaz; Project ID: 2012.1.00173.S, PI: J. S. Dunlop). After adopting a 250 kλ taper, which gives an optimal combination of the sensitivity and angular resolution, the final map reached a typical rms noise of 30 μJy beam^{-1} at the central $\sim$4 arcmin^2 and $\sim$70 μJy beam^{-1} at the remaining area with the synthesized beam $0\farcs59 \times 0\farcs53$ (PA $= -83°$).

Yamaguchi et al. (2019) report that 20 of 25 sources candidates have been listed in *K*-band selected sources catalog by the FourStar galaxy evolution survey (ZFOURGE; Straatman et al. 2016; the 5σ limiting magnitude of $K_s = 26.0$ mag at the 80% completeness levels). The ASAGAO sources are cross-matched against the ZFOURGE catalog, after correcting for a systematic offset with respect to the ALMA image ($-0\farcs086$ in R.A. and $+0\farcs282$ in decl.), which is calibrated by the positions of stars in the *Gaia* Data Release 1 Catalog (Gaia Collaboration et al. 2016). Here, we adopt the search radius $= 0\farcs5$ for point-like sources, which is comparable with the synthesized beam of the final ALMA map. Considering the number of ZFOURGE sources within the ASAGAO field ($\sim$3000), the likelihood of random coincidence is estimated to be 0.03 (this likelihood is often called the *p*-value; Downes et al. 1986). In the case that a counterpart is largely extended in the *K*-band image, we allow a larger positional offset, up to half-light radius of the *K*-band emission. However, we still have five candidates without ZFOURGE counterparts with S/N > 5, which are undetected at *K* band (Figure 1). We summarize the ASAGAO candidates without ZFOURGE counterparts in Table 1, and show the multi-wavelength postage stamps of these five near-IR-dark faint ALMA candidates in Figure 2.

We check the reliability of these near-IR-dark faint ALMA candidates using two independent methods. First, we apply the same source finding algorithm to the negative map to estimate the degree of contamination by spurious detections. The semi-analytical model by Casey et al. (2018) suggests that the contamination rate is small in the range of S/N > 5.0. There is no negative detections with S/N > 5.2 to be compared with the 23 positive detections with S/N > 5.2. In the $5.0 <$ S/N < 5.2 bin, we find one negative detections and two positive detections (i.e., ID24 and ID25; see Table 1). Therefore, the negative fraction in the S/N bin is 0.5 (see also Figure 15 in Hatsukade et al. 2018). Second, we split the ASAGAO visibilities into two polarization components (i.e., *XX* and *YY* polarization images) and create two *XX* and *YY* images, which are purely independent. With these two images, we find that all five candidates are detected with S/N $\sim$ 3–5 in both *XX* and *YY*. This is the behavior expected for $>5\sigma$ detections. On the basis of these tests, we suggest that two highest S/N near-IR-dark ALMA sources seem to be secure, whereas remaining three sources may contain false detections. To test the reality of these sources further, we then consult with other deep images available in the next section.

3. *K*-dropout ASAGAO Candidates

In this section, we describe ASAGAO candidates without ZFOURGE counterparts (hereafter, *K*-dropout ASAGAO candidates) individually. First, we perform a stacking analysis for each 5 *K*-dropout ASAGAO candidates using optical/near-IR images obtained by the 3D-*HST* survey (Grogin et al. 2011; Koekemoer et al. 2011; Skelton et al. 2014). This technique is often used to check reliability of extremely high-redshift ($z \gtrsim 7$) Lyman break galaxies (e.g., Bouwens et al. 2013). We use the Advanced Camera for Survey (ACS; Ford et al. 1998)/

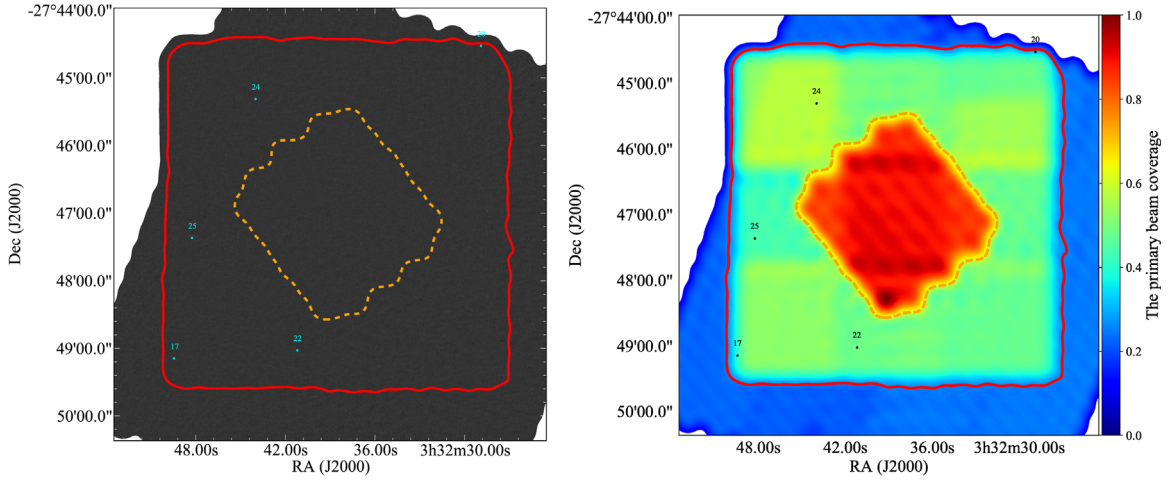

Figure 1. ASAGAO 1.2 mm continuum map of GOODS-S (left panel) and the PB coverage map (right panel). Here, we combined ASAGAO original data, HUDF data (Dunlop et al. 2017), and a part of the GOODS-S ALMA data (Franco et al. 2018). In this paper, we only consider the ASAGAO field indicated by the red solid line ($\sim 5' \times 5'$). The orange dashed line indicates the area covered by Dunlop et al. (2017). The cyan and black circles in the right and left panel indicate five near-IR-dark ASAGAO candidates, respectively.

Table 1
K-dropout ASAGAO Sources

ID (ASAGAO) (1)	R.A. (degree) (2)	Decl. (degree) (3)	$S_{\rm ALMA}$ (mJy) (4)	$S/N_{\rm peak}$ (5)	PB Coverage[a] (6)	$z_{3.6\ \mu m/1.2\ mm}$ (7)	$z_{5.0\ cm/1.2\ mm}$ (8)	Counterpart? (9)
17	53.206042	−27.819166	0.564 ± 0.090	6.078	0.403	$3.93^{+0.43}_{-0.30}$	>4.14	Y
20	53.120445	−27.742093	0.614 ± 0.109	5.565	0.317	>5.52	>4.39	Y
22	53.171662	−27.817153	0.612 ± 0.101	5.446	0.483	>5.41	>4.26	···
24	53.183284	−27.755207	0.446 ± 0.082	5.022	0.572	>4.48	>3.70	···
25	53.201002	−27.789483	0.858 ± 0.223	5.020	0.438	>5.92	>4.93	···

Notes. Columns: (1) ASAGAO ID. (2) R.A. (J2000). (3) Decl. (J2000). (4) Spatial integrated flux density (de-boosted). (5) Peak S/N. (6) The PB coverage at the position of *K*-dropout ASAGAO sources (see Figure 1). (7) and (8) The photometric redshifts estimated by the flux ratios between 3.6 μm and 1.2 mm and 5.0 cm and 1.2 mm, respectively. Here, we assume the average SED of ALESS sources with $A_V > 3.0$ (see Section 4). (9) Based on the cross-matching with catalogs by Ashby et al. (2015) and Cowie et al. (2018); "Y" is assigned if *K*-dropout ASAGAO sources have counterparts at *Spitzer*/IRAC, JCMT/SCUBA2, or ALMA Band 7. As discussed in Section 3, ID17 and ID20 are secure detections, and the rest of three are treated as rather tentative.

[a] The primary beam (PB) coverage values in Table 1 look smaller than typical values (>0.5), but this does not mean that these are sources outside nominal fields of view (FoVs); this is simply caused by the nonuniform PB coverage of the ASAGAO final map (Figure 1, right panel), which was produced by combining three different ALMA programs including the HUDF data (Dunlop et al. 2017), and the GOODS-S ALMA data (Franco et al. 2018), as well as the ASAGAO data. If we exclude the HUDF data, which cause the nonuniformity (the orange dashed region in Figure 1), the PB coverage value of ID17, ID20, ID22, ID24, and ID25 is 0.62, 0.48, 0.79, 0.97, and 0.69, respectively.

F435W, *F606W*, *F775W*, *F850LP*, *F814W*, and the Wide Field Camera 3 (WFC3; Kimble et al. 2008)/*F125W*, *F140W*, *F160W*.[25] In the stacking analysis, the point-spread functions (PSFs) of the *Hubbel Space Telescope* (*HST*) images are matched to the WFC3/*F160W* image ($\simeq 0\farcs16$). We show the results of the stacking in Figure 3. We find no significant detections even in these ACS/WFC3 stacked images. Nevertheless, we find that two of the K-dropout ASAGAO candidates have independent detections in longer wavelengths as follows:

1. *ID*17. This object is detected at 3.6 and 4.5 μm bands of *Spitzer*/InfraRed Array Camera (IRAC; Fazio et al. 2004) by the *Spitzer*-Cosmic Assembly Deep Bear infrared Extragalactic Legacy Survey (S-CANDELS; PI G.Fazio; Ashby et al. 2015, see Figure 2). Its apparent magnitudes at 3.6 and 4.5 μm are 25.38 ± 0.30 and 25.00 ± 0.27 mag, respectively (Ashby et al. 2015).
2. *ID*20. This object is detected at JCMT/SCUBA2 and ALMA Band 7 (Cowie et al. 2018). The observed flux density is 1.35 ± 0.24 mJy at 870 μm (Cowie et al. 2018). This source is recognized as ID68 in Cowie et al. (2018).

Considering the multiwavelength information, two of the five *K*-dropout ASAGAO candidates with multiwavelength counterparts (i.e., ID17 and ID20) must be real (secure detections), while we suggest that the rest of three candidates without multiwavelength counterparts should remain "candidates," which shall be verified by further follow-up observations.

4. Physical Properties

These extremely red colors can be reproduced by the high-redshift sources or highly reddened low-redshift sources (e.g.,

[25] These images are available at the 3D-*HST* website: https://3dhst.research.yale.edu/Data.php.

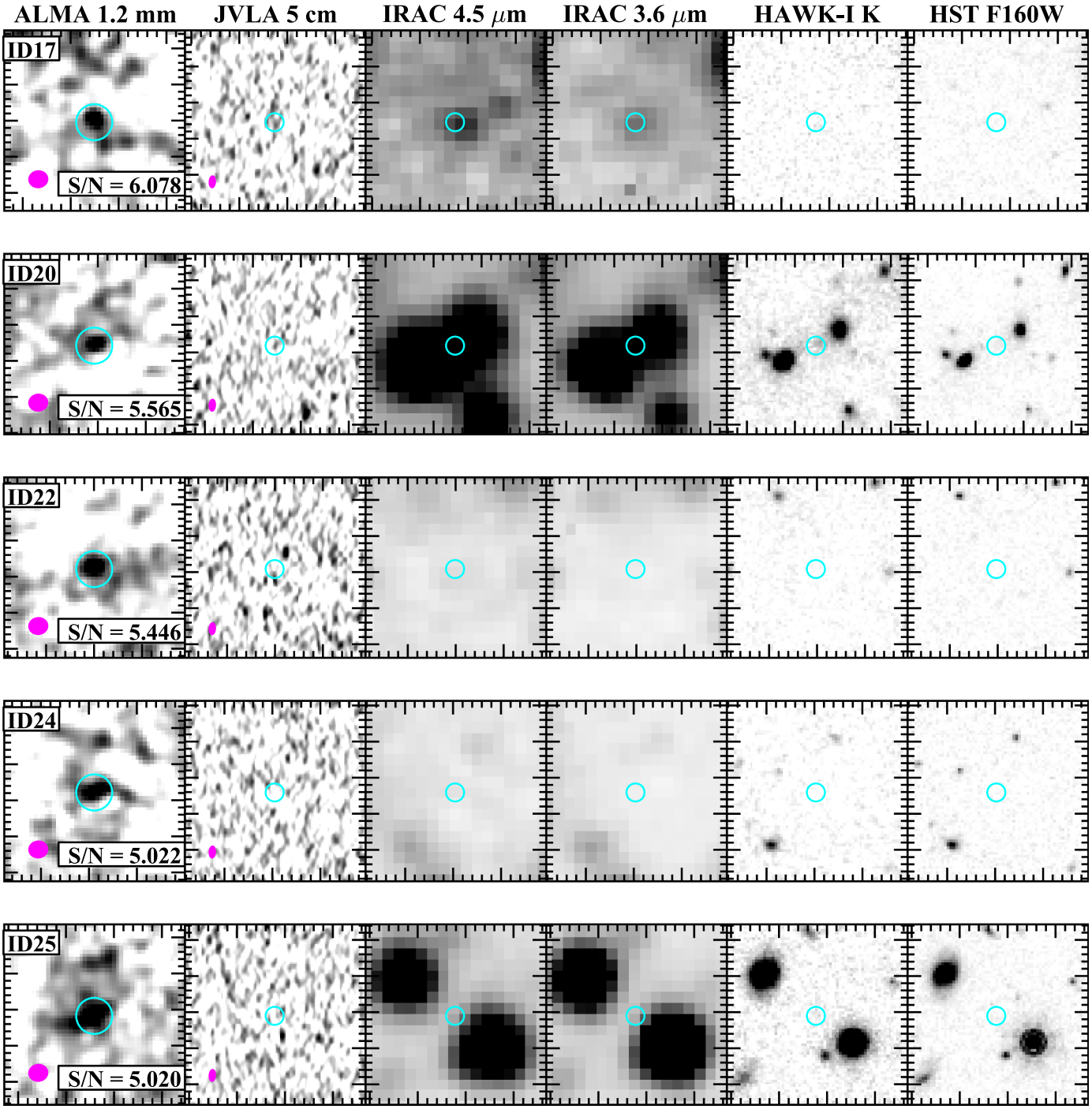

Figure 2. Multiwavelength images of ASAGAO candidates without *K*-band counterparts. From left to right: ALMA 1.2 mm ($5'' \times 5''$), JVLA 5 cm, *Spitzer* IRAC/4.5 μm, IRAC/3.6 μm, VLT HAWK-I/K_s, and *HST*) WFC3/*F*160*W* images ($10'' \times 10''$). The cyan circles are $1''$ apertures. The inserted S/N values are those of ALMA data. The magenta symbols are the synthesized beam of ALMA and JVLA.

Caputi et al. 2012). We plot optical-to-radio spectral energy distributions (SEDs) of these *K*-dropout ASAGAO sources (including three candidates) in Figure 4. As a comparison, we also show the average SED of ALESS[26] sources with visual extinction (A_V) > 3.0 (the reddest case; hereafter, we call this SED as the average SED of ALESS SMGs) obtained by da Cunha et al. (2015). As shown in Figure 4, all sources can lie at $z \gtrsim 3$–5, even though we assume the highly reddened SED. The relation between the flux ratio between 3.6 μm and 1.2 mm ($S_{3.6\ \mu m}/S_{1.2\ mm}$; the left panel of Figure 5) also prefer high-redshift cases. For ID17 which is detected at 3.6 μm, the ratio indicates that it can lie at $z = 3.93^{+0.43}_{-0.30}$, when we assume the average SED of ALESS sources. The redshift error is attributed to the error in the $S_{3.6\ \mu m}/S_{1.2\ mm}$ ratio. On the other hand, as shown in the left panel of Figure 5, variation between SEDs are quite large and some degeneracy between the reddened-color and redshift is still unresolved at 3.6 μm.

[26] The ALMA follow-up observation of the LABOCA Extended *Chandra* Deep Field South Survey (e.g., Hodge et al. 2013; Swinbank et al. 2014; da Cunha et al. 2015).

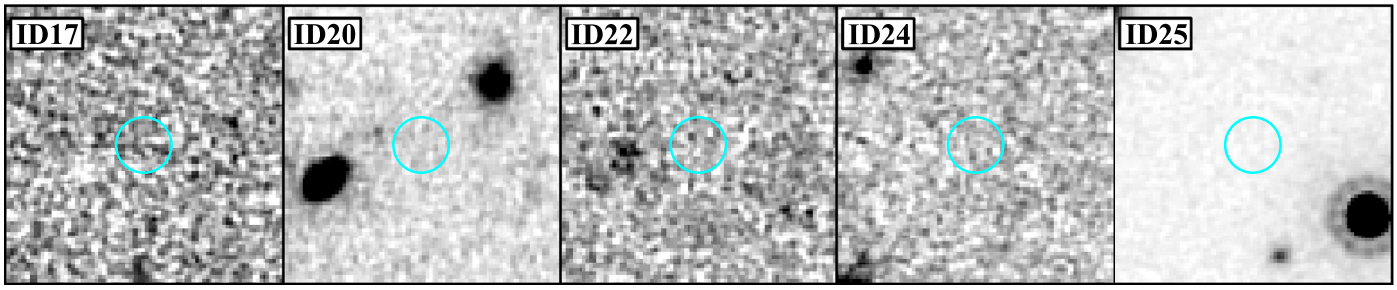

Figure 3. Stacked *HST* images for K-dropout ASAGAO candidates ($5'' \times 5''$). The cyan circles indicate ALMA positions (radius $= 0\farcs5$).

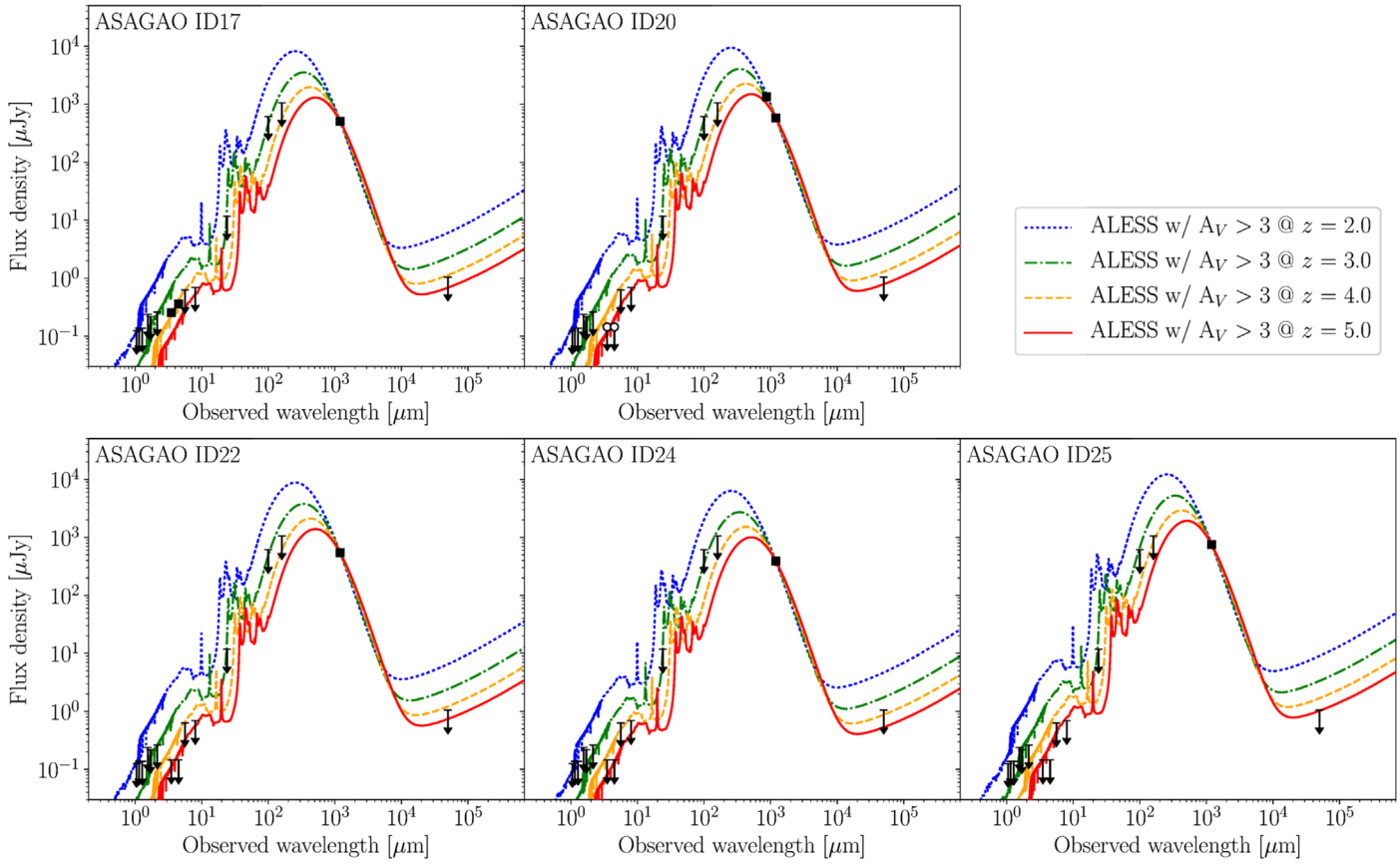

Figure 4. Optical-to-radio SED of ASAGAO sources without *K*-band counterparts. Black arrow indicate 3σ upper limits. From optical-to far-IR upper limits except for IRAC 5.6 and 8.0 μm are listed in Straatman et al. (2016). The upper limits at IRAC 5.6 and 8.0 μm are presented in Dickinson et al. (2003). The radio image at 5 cm is obtained by JVLA (W. Rujopakarn et al. 2019, in preparation). For ID20, we also plot its ALMA Band 7 flux density. We have to note that we should not refer upper limits at *Spitzer*/IRA*C* bands of ID20 (white open circles with upper limits) because of the contamination from nearby sources (Figure 2). The blue dotted line, green dotted–dashed line, orange dashed line, and red solid line indicate the average SED of ALESS sources with $A_V > 3.0$ at $z = 2$, 3, 4, and 5, respectively (da Cunha et al. 2015). Note that these SEDs are scaled to their observed flux densities at ALMA wavelength.

They are not detected by the Kerl G. Jansky Very Large Array (JVLA) *C* band (5 cm) deep observation ($\sigma \simeq 0.35$ μJy beam^{-1}; Rujopakarn et al. 2016; W. Rujopakarn et al. 2019, in preparation). As suggested by Carilli & Yun (1999), the flux ratio between radio and (sub-)millimeter wavelengths can be a redshift indicator. In the right panel of Figure 5, we show the redshift dependence of the flux ratio at radio and millimeter wavelengths ($S_{5\,\mathrm{cm}}/S_{1.2\,\mathrm{mm}}$). We show the upper limits of the flux ratio of *K*-dropout ASAGAO sources including 3 candidates. As comparisons, we also plot the redshift dependence of $S_{5\,\mathrm{cm}}/S_{1.2\,\mathrm{mm}}$ of IR bright sources. The result suggests that their flux ratio are roughly consistent with the estimated redshifts (i.e., $z \gtrsim 3$–5) when we assume the average SED of ALESS sources. In Table 1, we show the estimated lower limits of photometric redshifts in this case.

In the high-redshift case (i.e., $z \sim 4$), the 3σ upper limits of stellar masses of *K*-dropout ASAGAO sources are estimated to be $\log(M_*/M_\odot) \lesssim 10.4$ using *Spitzer*/IRAC 8.0 μm, i.e., rest-frame *H*-band data (3σ limiting magnitude of 24.3 mag; Dickinson et al. 2003) if they lie at $z \sim 4$. Here, we assume a mass-to-light ratio obtained in the rest-frame *H*-band luminosity (e.g., Hainline et al. 2011). Hainline et al. (2011) estimated the mass-to-light ratio of dusty sources $M_*/L_H = 0.17$ and 0.13 $M_\odot L_\odot^{-1}$ for constant and single-burst star formation histories, respectively. In this paper, we adopt the average value (i.e., $M_*/L_H = 0.15\ M_\odot\ L_\odot^{-1}$) of those two extreme case. We also estimate its IR luminosity by integrating the SED

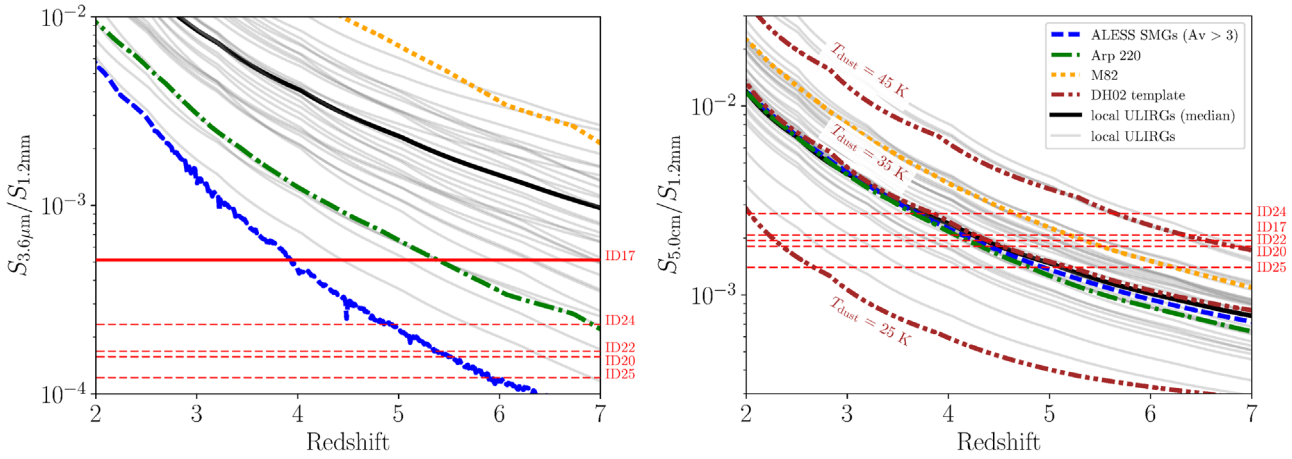

Figure 5. Redshift dependence of $S_{3.6\ \mu m}/S_{1.2\ mm}$ (left panel) and $S_{5\ cm}/S_{1.2\ mm}$ (right panel) flux ratios. The blue dashed line, green dotted–dashed line, and orange dotted line indicates the average SED of ALESS sources with $A_V > 3.0$ (da Cunha et al. 2015), Arp 220, and M82 (Silva et al. 1998), respectively. Gray solid lines are local ULIRGs compiled by Vega et al. (2008) and the black solid line is the median of these ULIRGs. Brown chain double dashed line in the right panel is SED templates of Dale & Helou (2002) with dust temperature, $T_{dust} = 25$, 35, and 45 K. The horizontal red solid line in the left panel is the $S_{3.6\ \mu m}/S_{1.2\ mm}$ value of ID17. Horizontal red lines in the left and right panels are the upper limit of $S_{3.6\ \mu m}/S_{1.2\ mm}$ (the left panel) and $S_{5\ cm}/S_{1.2\ mm}$ (the right panel) flux ratios of ASAGAO *K*-dropout sources.

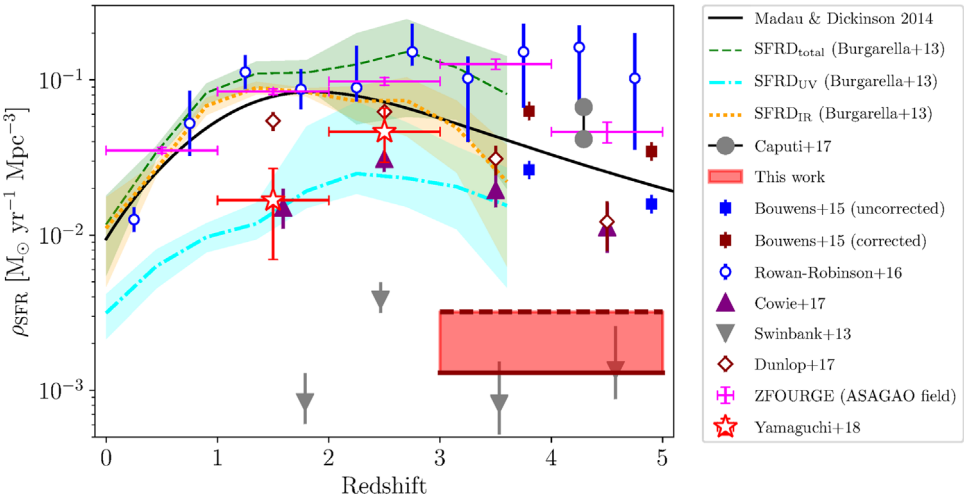

Figure 6. Contribution of ASAGAO sources to the cosmic SFRD as a function of redshift. The red shaded area indicates the contribution of *K*-drop ASAGAO sources. The horizontal solid line corresponds to the SFR density computed by two secure *K*-dropout ASAGAO sources. The dashed line in the red shaded region indicate the range of SFRD when remaining 3 candidates are also real, respectively (see Section 5 for details). Red open symbols and magenta symbols are the contributions of ASAGAO sources with *K*-band counterparts and ALMA non-detected ZFOURGE sources within ASAGAO field respectively (Yamaguchi et al. 2019). The black solid line indicate the recent results of the redshift evolution of the cosmic SFRD obtained by Madau & Dickinson (2014). The green dashed line, cyan dotted–dashed line, and orange dotted line show the total (i.e., UV + IR) SFRD, UV SFRD, and IR SFRD obtained by Burgarella et al. (2013). Blue and brown squares are dust-uncorrected and -corrected SFRD obtained by Bouwens et al. (2015). Blue open circles are results of Rowan-Robinson et al. (2016). Purple triangles indicate the cosmic SFRD obtained by the SCUBA2 large survey Cowie et al. (2017). Gray inverse-triangle are the contribution of bright ALESS sources (Swinbank et al. 2014). Gray filled circles are lower and upper limit of the contribution of Hα emitters obtained by Caputi et al. (2017). Brown open diamonds indicate the contribution of the ALMA sources obtained by Dunlop et al. (2017). We note that these results are converted to the Chabrier IMF.

presented in Figure 4 and find $\log(L_{IR}/L_\odot) \sim 12.0$ corresponding to $\log(SFR/[M_\odot\ yr^{-1}]) \sim 2$. Here, we assume the average SED of ALESS sources at $z \sim 4$. When we consider the M_*–SFR relation at $z \sim 4$ (e.g., Schreiber et al. 2017), they show starburst-like features. As discussed in Wang et al. (2016), this source can represent the early phase of formation of massive galaxies, which are difficult to be observed using rest-frame ultraviolet (UV) selected galaxies such as Lyα emitters or Lyman break galaxies.

In the low-redshift case (i.e., $z \sim 2$), we can estimate the stellar mass of ID17 to be $\log(M_*/M_\odot) \simeq 9.4$, because it is detected at *Spitzer*/IRAC 4.5 μm data, which delivers the rest-frame *H*-band light at $z \sim 2$. According to Straatman et al. (2016), a completeness limit of the ZFOURGE survey is $\log(M_*/M_\odot) \sim 9.0$ at $z = 2$, which implies that ID17 prefers the high-redshift case rather than the low-redshift case. For other 4 *K*-dropout ASAGAO sources including 3 candidates, their 3σ upper limits of stellar masses are estimated to be $\log(M_*/M_\odot) \lesssim 8.8$ when we consider the 3σ limiting magnitude of S-CANDELS (26.5 mag).[27] These upper limits are consistent with their non-detections at *K* band. Thus, we can not exclude the low-redshift case for these 4 sources. If they lie at $z \sim 2$, their IR luminosities are estimated to be $\log(L_{IR}/L_\odot) \sim 11.6$ when we assume the SED template of Dale & Helou (2002) with $T_{dust} = 25$ K. Therefore, in this

[27] For ID20, it is difficult to use *Spitzer*/IRAC photometries because of heavy confusions (Figure 2).

case, they seem to be extremely low-mass starburst galaxies, which have been missed in previous deep surveys at optical/near-IR wavelengths.

5. Contribution to the Cosmic SFRD

Many previous studies predict that the contribution of dust-obscured star-forming activities to the cosmic SFRD have a peak level at $z \simeq 2$–3 and decline toward $z \gtrsim 3$–4 based on, for example, IR luminosity functions obtained by the *Herschel* (e.g., Burgarella et al. 2013) or dust attenuation-corrected UV observations (e.g., Bouwens et al. 2015). On the other hand, Rowan-Robinson et al. (2016) predict that the contribution seems to be constant at $z = 1$–5 based on the integrated SFR functions estimated by *Hershel*/SPIRE-500 μm sources.

According to Simpson et al. (2014), their optical/near-IR-dark SMGs are located in the redshift range of $z \sim 3$–5. Thus, in this section, we assume the case that all of *K*-dropout ASAGAO candidates lie somewhere in the redshift interval of $z \sim 3$–5. When we use the average SED of ALESS sources, their contribution to the cosmic IR SFRD is estimated to be $\rho_{\rm SFR} \sim (1\text{–}3) \times 10^{-3}\,M_{\odot}\,{\rm yr}^{-1}\,{\rm Mpc}^{-3}$, which corresponding to ~10%–30% of previous works (e.g., Madau & Dickinson 2014). Here, we simply sum up the SFRs of *K*-dropout ASAGAO sources and divide them by the co-moving volume. The uncertainty of their contributions to the cosmic IR SFRD in Figure 6 are attributable to the relativity of *K*-dropout ASAGAO candidates. If only 2 secure sources with counterparts (i.e., ID17 and ID20) are real, their contribution is expressed by the solid horizontal dark-red line in Figure 6 ($\rho_{\rm SFR} \sim 1 \times 10^{-3}\,M_{\odot}\,{\rm yr}^{-1}\,{\rm Mpc}^{-3}$). On the other hand, in the case that all 5 sources are real, their contribution is shown by the dark-red dashed horizontal line ($\rho_{\rm SFR} \sim 3 \times 10^{-3}\,M_{\odot}\,{\rm yr}^{-1}\,{\rm Mpc}^{-3}$).

We also consider uncertainty attributed to different assumed SEDs. If we estimated SFRs of *K*-dropout ASAGAO candidates using SED templates presented in Figure 5, their contributions to the cosmic IR SFRD can vary by ~±0.3 dex, which dose not affect following our conclusion significantly.

As shown in Figure 6, their contributions to the cosmic SFRD can be comparable with, or greater than that of bright ALESS SMGs ($S_{870\,\mu{\rm m}} > 4.2$ mJy; Swinbank et al. 2014). Therefore, the non-negligible contribution of dust-obscured star formation activities to the cosmic SFRD at high redshift could have been missed in previous surveys. This result shows the importance of ALMA deep contiguous survey to study the evolution of the cosmic SFRD.

We thank the referee for the comments, which improved the manuscript. This paper makes use of the following ALMA data: ADS/JAO.ALMA#2015.1.00098.S, 2015.1.00543.S, and 2012.1.00173.S. ALMA is a partnership of ESO (representing its member states), NSF (USA), and NINS (Japan) together with NRC (Canada), NSC and ASIAA (Taiwan), and KASI (Republic of Korea) in cooperation with the Republic of Chile. The Joint ALMA Observatory is operated by ESO, AUI/NRAO, and NAOJ. Data analysis was partly carried out on the common-use data analysis computer system at the Astronomy Data Center (ADC) of the National Astronomical Observatory of Japan. Y. Yamaguchi is thankful for the JSPS fellowship. This study was supported by the JSPS Grant-in-Aid for Scientific Research (S) JP17H06130 and the NAOJ ALMA Scientific Research Number 2017-06B.

ORCID iDs

Yuki Yamaguchi https://orcid.org/0000-0002-7019-4010
Kotaro Kohno https://orcid.org/0000-0002-4052-2394
Bunyo Hatsukade https://orcid.org/0000-0001-6469-8725
Tao Wang https://orcid.org/0000-0002-2504-2421
Yiping Ao https://orcid.org/0000-0003-3139-2724
Karina I. Caputi https://orcid.org/0000-0001-8183-1460
Daniel Espada https://orcid.org/0000-0002-8726-7685
Seiji Fujimoto https://orcid.org/0000-0001-7201-5066
Rob J. Ivison https://orcid.org/0000-0001-5118-1313
Tadayuki Kodama https://orcid.org/0000-0002-2993-1576
Haruka Kusakabe https://orcid.org/0000-0002-3801-434X
Tohru Nagao https://orcid.org/0000-0002-7402-5441
Masami Ouchi https://orcid.org/0000-0002-1049-6658
Wiphu Rujopakarn https://orcid.org/0000-0002-0303-499X
Ken-ichi Tadaki https://orcid.org/0000-0001-9728-8909
Yoichi Tamura https://orcid.org/0000-0003-4807-8117
Yoshihiro Ueda https://orcid.org/0000-0001-7821-6715
Hideki Umehata https://orcid.org/0000-0003-1937-0573
Wei-Hao Wang https://orcid.org/0000-0003-2588-1265
Min S. Yun https://orcid.org/0000-0001-7095-7543

References

Aravena, M., Decarli, R., Walter, F., et al. 2016, ApJ, 833, 68
Ashby, M. L. N., Willner, S. P., Fazio, G. G., et al. 2015, ApJS, 218, 33
Bouwens, R. J., Illingworth, G. D., Oesch, P. A., et al. 2015, ApJ, 803, 34
Bouwens, R. J., Oesch, P. A., Illingworth, G. D., et al. 2013, ApJL, 765, L16
Burgarella, D., Buat, V., Gruppioni, C., et al. 2013, A&A, 554, A70
Caputi, K. I., Deshmukh, S., Ashby, M. L. N., et al. 2017, ApJ, 849, 45
Caputi, K. I., Dunlop, J. S., McLure, R. J., et al. 2012, ApJL, 750, L20
Carilli, C. L., & Yun, M. S. 1999, ApJL, 513, L13
Casey, C. M., Hodge, J., Zavala, J. A., et al. 2018, ApJ, 862, 78
Chabrier, G. 2003, PASP, 115, 763
Cowie, L. L., Barger, A. J., Hsu, L.-Y., et al. 2017, ApJ, 837, 139
Cowie, L. L., González-López, J., Barger, A. J., et al. 2018, ApJ, 865, 106
da Cunha, E., Walter, F., Smail, I. R., et al. 2015, ApJ, 806, 110
Dale, D. A., & Helou, G. 2002, ApJ, 576, 159
Dickinson, M., Giavalisco, M. & GOODS Team 2003, in The Mass of Galaxies at Low and High Redshift, ed. R. Bender & A. Renzini (Berlin: Springer), 324
Downes, A. J. B., Peacock, J. A., Savage, A., & Carrie, D. R. 1986, MNRAS, 218, 31
Dunlop, J. S., McLure, R. J., Biggs, A. D., et al. 2017, MNRAS, 466, 861
Fazio, G. G., Hora, J. L., Allen, L. E., et al. 2004, ApJS, 154, 10
Ford, H. C., Bartko, F., Bely, P. Y., et al. 1998, Proc. SPIE, 3356, 234
Franco, M., Elbaz, D., Béthermin, M., et al. 2018, A&A, 620, A152
Fujimoto, S., Ouchi, M., Kohno, K., et al. 2018, ApJ, 861, 7
Fujimoto, S., Ouchi, M., Ono, Y., et al. 2016, ApJS, 222, 1
Gaia Collaboration, Brown, A. G. A., Vallenari, A., et al. 2016, A&A, 595, A2
Grogin, N. A., Kocevski, D. D., Faber, S. M., et al. 2011, ApJS, 197, 35
Hainline, L. J., Blain, A. W., Smail, I., et al. 2011, ApJ, 740, 96
Hatsukade, B., Kohno, K., Umehata, H., et al. 2016, PASJ, 68, 36
Hatsukade, B., Kohno, K., Yamaguchi, Y., et al. 2018, PASJ, 70, 105
Hodge, J. A., Karim, A., Smail, I., et al. 2013, ApJ, 768, 91
Kimble, R. A., MacKenty, J. W., O'Connell, R. W., & Townsend, J. A. 2008, Proc. SPIE, 7010, 70101E
Koekemoer, A. M., Faber, S. M., Ferguson, H. C., et al. 2011, ApJS, 197, 36
Kohno, K., Yamaguchi, Y., Tamura, Y., et al. 2016, Galaxies at High Redshift and Their Evolution Over Cosmic Time, in Proc. IAU Symp. 319, ed. S. Kaviraj (Cambridge: Cambridge Univ. Press), 92
Madau, P., & Dickinson, M. 2014, ARA&A, 52, 415
Rowan-Robinson, M., Oliver, S., Wang, L., et al. 2016, MNRAS, 461, 1100
Rujopakarn, W., Dunlop, J. S., Rieke, G. H., et al. 2016, ApJ, 833, 12
Schreiber, C., Pannella, M., Leiton, R., et al. 2017, A&A, 599, A134
Silva, L., Granato, G. L., Bressan, A., & Danese, L. 1998, ApJ, 509, 103
Simpson, J. M., Smail, I., Swinbank, A. M., et al. 2015, ApJ, 807, 128
Simpson, J. M., Swinbank, A. M., Smail, I., et al. 2014, ApJ, 788, 125
Skelton, R. E., Whitaker, K. E., Momcheva, I. G., et al. 2014, ApJS, 214, 24
Straatman, C. M. S., Spitler, L. R., Quadri, R. F., et al. 2016, ApJ, 830, 51
Swinbank, A. M., Simpson, J. M., Smail, I., et al. 2014, MNRAS, 438, 1267

Tadaki, K.-i., Kohno, K., Kodama, T., et al. 2015, ApJL, 811, L3
Tamura, Y., Iono, D., Wilner, D. J., et al. 2010, ApJ, 724, 1270
Ueda, Y., Hatsukade, B., Kohno, K., et al. 2018, ApJ, 853, 24
Vega, O., Clemens, M. S., Bressan, A., et al. 2008, A&A, 484, 631
Wang, T., Elbaz, D., Schreiber, C., et al. 2016, ApJ, 816, 84
Wang, W.-H., Barger, A. J., & Cowie, L. L. 2009, ApJ, 690, 319
Wang, W.-H., Kohno, K., Hatsukade, B., et al. 2016, ApJ, 833, 195
Yamaguchi, Y., Kohno, K., Hatsukade, B., et al. 2019, ApJ, submitted
Yamaguchi, Y., Tamura, Y., Kohno, K., et al. 2016, PASJ, 68, 82
Yun, M. S., Aretxaga, I., Ashby, M. L. N., et al. 2008, MNRAS, 389, 333